


RESEARCH ARTICLE

Atomic configuration, electronic structure, and work of adhesion of TiN(111)//B2-NiTi(110) and TiN(111)//B19'-NiTi(010) interfaces: Insights from first-principles simulations

Dong Xie¹  | Xiaoting Wang¹ | Longjun Wei² | Ran Zhang¹ |
Rajesh Ganesan^{3,4} | David T. A. Matthews⁵ | Yongxiang Leng²

¹Key Laboratory of Advanced Technologies of Materials, Ministry of Education of China, School of Physical Science and Technology, Southwest Jiaotong University, Chengdu, China

²School of Materials Science and Engineering, Southwest Jiaotong University, Chengdu, China

³The University of Sydney, Sydney, NSW, Australia

⁴Department of Nuclear, Plasma, and Radiological Engineering, Center for Plasma-Material Interactions, University of Illinois at Urbana-Champaign, Urbana, IL, USA

⁵Department of Mechanics Solids and Surfaces, Faculty of Engineering Technology, University of Twente, Enschede, The Netherlands

Correspondence

Dong Xie, Key Laboratory of Advanced Technologies of Materials, Ministry of Education of China, School of Physical Science and Technology, Southwest Jiaotong University, Chengdu 610031, China.
Email: xiedong@home.swjtu.edu.cn

Yongxiang Leng, School of Materials Science and Engineering, Southwest Jiaotong University, Chengdu 610031, China.
Email: yxleng@263.net

Funding information

Natural Science Foundation of Sichuan Province, China, Grant/Award Number: 2022NSFSC0292

In this paper, the atomic configuration, electronic structure, and work of adhesion for TiN(111)//B2-NiTi(110) and TiN(111)//B19'-NiTi(010) interfaces were investigated by first-principles calculations based on density functional theory (DFT), which aim to provide a theoretical guidance for analyzing the service reliability of TiN films modified NiTi alloy devices. The results of this paper indicated that a hollow-site stacking structure was formed on the interface when Ti and N were the terminal atoms on two sides. Such interfaces demonstrated a stronger bonding performance and a more stable structure than that with Ni and Ti as the terminal atoms. The work of adhesion of the TiN(111)//B19'-NiTi(010) interface was 17.47 J/m², which is greater than the work of fracture of TiN(111) (6.73 J/m²), whereas the work of adhesion of the TiN(111)//B2-NiTi(110) interface was found to reach 5.49 J/m², which is lower than the work of fracture of TiN(111). The models of the work of adhesion between the two interfaces indicate that there are significant bond strength changes in the TiN/NiTi interface, when the NiTi substrate undergoes martensitic transformation. The results of this paper contribute significantly to the service reliability analysis of TiN films coated on NiTi alloy devices.

KEYWORDS

electronic structure, NiTi shape memory alloy, TiN films, work of adhesion

1 | INTRODUCTION

NiTi shape memory alloys (SMAs) have been extensively applied in biomedicine,¹ microelectromechanical systems (MEMS),² aerospace,³ and robots,⁴ owing to their specific shape memory and hyperelastic bulk properties. Further improvements of these SMAs can be achieved through surface functionalization by applying advanced coatings.

Typical surface engineering techniques studied for NiTi SMAs up to now include surface oxidation, ion plating, magnetron sputtering, sol-gel, and other ionic spraying methods. The resulting coatings include TiO₂,^{5,6} TiN,⁷ SiO₂,⁸ and Ti-Ta⁹ films, aimed at improving the biocompatibility, corrosion resistance, and/or wear resistance of NiTi products.

As the design of NiTi alloy devices inherently exploits the superelasticity and shape memory function of the material, these devices will

inevitably deform to various degrees during service. Therefore, for the product performance of coated SMA systems, the interfacial bond strength between the coatings and the substrate is critical. The shape memory and superelasticity of NiTi alloys are attributed to the reversible martensitic phase transformation.¹⁰ During martensitic phase transformation, the NiTi alloy transforms from the austenite phase (body-centered cubic B2 structure) to the martensite phase (monoclinic B19' structure), which inevitably modifies the film/NiTi interface structure and interface bonding; however, these physicochemical changes occur at the interface and are considerably difficult to observe or analyze in the laboratory. Some studies have reported the deformation and failure of TiO₂ films on the surface of NiTi, which undergo hyperelasticity and shape memorization deformation.^{6,11} However, research on the effect of NiTi phase transformation to film/substrate interface bond and the failure mechanism from atomic or electronic scales have rarely been reported.

Owing to significant advancements in calculation and simulation technologies, more researchers have started to adopt the first-principles method to investigate the structure and bonding performance of interfaces. Through first-principles calculations, the electronic structure and bonding of interfaces can be analyzed, and the results can improve the essential knowledge on the bonding or failure of film/substrate interfaces in coatings design and product performance. Some studies have focused on first-principles research related to the NiTi alloy/coating interface. For example, Chen et al.¹² calculated the bond strength and fracture mechanism of the NiTi (111)//a-Al₂O₃ (0001) interface; Hong-Li et al.¹³ studied the effect of Nb doping on the electronic structure of the TiO₂//NiTi interface; and Li et al.¹⁴ simulated the structural features of the NiTi//Nb interface. However, these studies considered only the B2 phase structure as a substrate, whereas in actual applications, NiTi transforms between the B2 structure and the monoclinic phase B19' structure under stress or temperature. However, the physicochemical modifications in the film/NiTi interfaces with B19'-NiTi as a substrate have not been investigated or simulated yet.

This study focused on the application of a NiTi alloy device modified by a TiN film. The TiN(111) surface was combined with the B2 phase structure NiTi(110) surface (hereafter mentioned as B2-NiTi (110)) and the monoclinic phase B19' structure NiTi(010) surface

(hereafter mentioned as B19'-NiTi(010)), to construct the following two interface models: TiN(111)//B2-NiTi(110) and TiN(111)//B19'-NiTi(010), respectively. Furthermore, CASTEP, a simulation package based on density functional theory (DFT),¹⁵ was used to compute electronic structure, charge density, Mulliken population, work of adhesion, and the work of fracture of these two interfaces. The selected TiN(111), B2-NiTi(110), and B19'-NiTi(010) possessed densely packed atomic surfaces in their respective crystal textures, which is a surface with the lowest surface energy and the most stable structure. The current study aims to help us understand the changes in the film/NiTi interface structure and the bonding performance of NiTi before and after martensitic transformation, which is of significant importance for the service reliability analysis of TiN films modified NiTi alloy devices.

2 | CALCULATION MODEL AND METHOD

In the calculation for the NiTi alloy of the B2 phase structure¹⁶ (hereafter referred to as B2-NiTi), the space group was Pm-3m (group number 221); for NiTi alloy of the B19' phase structure¹⁷ (hereafter, B19'-NiTi), the space group was P21/M (group number 11). TiN exhibited a cubic structure, and the space group was Fm-3m (group number 225).¹⁸ Experimental unit cell parameters as were adopted for modeling are given in Table 1.

The TiN/NiTi interface model was constructed as follows: First, the geometric structure of B2-NiTi, B19'-NiTi, and TiN was optimized (Table 1). Second, B2-NiTi(110), B19'-NiTi(010), and TiN(111) surfaces were cut from the optimized crystal cell of B2-NiTi, B19'-NiTi, and TiN, respectively. To obtain a stable surface structure, convergence tests were conducted on the atomic layers of the surface structure of B2-NiTi(110), B19'-NiTi(010), and TiN(111). The surface energy of B2-NiTi(110), B19'-NiTi(010), and TiN(111) with different numbers of atomic layers was calculated, until the surface energy converged toward a stable value (deviation < 0.02 eV). Finally, the B2-NiTi(110), B19'-NiTi(010), and TiN(111) with optimized layers were combined to construct two interface models: TiN(111)//B2-NiTi(110) and TiN(111)//B19'-NiTi(010). To eliminate the interaction between each slab, a vacuum layer of thickness 10 Å was added in the interface

Structure	Methods or references		a (Å)	b (Å)	c (Å)
B2-NiTi	Current study	GGA-PBE	3.011	3.011	3.011
	Other calculations	GGA-PBE ¹⁹	3.005	3.005	3.005
	Experiment	Strutt et al. ²⁰	2.998	2.998	2.998
B19'-NiTi	Current study	GGA-PBE	4.932	4.011	2.932
	Other calculations	GGA-PBE ²¹	4.813	4.121	3.007
	Experiment	Otsuka and Ren ¹⁰	4.622	4.120	2.889
TiN	Current study	GGA-PBE	4.249	4.249	4.249
	Other calculations	GGA-PBE ²²	4.270	4.270	4.270
	Experiment	Kutschej et al. ²³	4.240	4.240	4.240

TABLE 1 Calculated and experimental values of the lattice constants of B2-NiTi, B19'-NiTi, and TiN

Abbreviation: GGA-PBE, general gradient approximation of Perdew–Burke–Ernzerhof.

models. In addition, when different surfaces were combined to form an interface, the lattice mismatch of the interface was ensured to be <5% through surface restructuring and unit cell expansion. Within the same interface model, there were many different interface structures because of the different terminal atoms. All possible interface structures, their charge density, work of adhesion, and Mulliken population were calculated in this paper.

In this study, all the calculations were performed using the CASTEP package, based on the DFT.¹⁵ General gradient approximation of Perdew–Burke–Ernzerhof (GGA-PBE) was adopted to determine the correlation energy of the electronic exchange. Then, ultrasoft pseudopotentials (USPP) was employed to define the electrons–ions interactions. Plane-wave basis vector groups were adopted for electron wave functions. The energy cut-off of the plane wave was set to 500 eV and the K-point spacing in the Brillouin zone was set to 0.02/Å based on the convergence test results of the total energy of the unit cells. For the self-consistent calculations, the convergence precision was set to 2.0×10^{-6} eV/atom, whereas the stress on each atom was restricted to <0.1 eV/nm, and the tolerance and stress deviations were limited to $<5.0 \times 10^{-5}$ nm and 20 MPa, respectively. Table 1 shows that the calculated unit cell parameters of NiTi and TiN were only slightly different from those in existing literature and experimental results, which indicates that the parameters selected in this study were highly reasonable.

3 | RESULTS AND DISCUSSION

3.1 | Surface structure, surface energy, and work of fracture

Figure 1A–C shows the surface structures of B2-NiTi(110), B19'-NiTi(010), and TiN(111), respectively. As shown in Figure 1A,B, each atomic layer contains equal Ni and Ti atoms in the surface structures of B2-NiTi(110) and B19'-NiTi(010). For B2-NiTi(110) and B19'-NiTi(010), the calculation formula of surface energy, γ_{surf} , is given as²⁴

$$\gamma_{\text{surf}} = \frac{E_{\text{slab}} - \left(\frac{n_{\text{slab}}}{n_{\text{bulk}}}\right)E_{\text{bulk}}}{2A}, \quad (1)$$

where E_{slab} , E_{bulk} , n_{slab} , n_{bulk} , and A denote the total energy of the surface structure, energy of the bulk unit cell structure, number of atoms in the surface structure, number of atoms in the bulk unit cell structure, and the area of the surface, respectively.

Figure 1C shows that in the surface structure of TiN(111), each atomic layer contains only either Ni or Ti atoms. If the surface structure contains an even number of atomic layers, it conforms to the stoichiometric chemical ratio; however, there are different types of terminal atoms at the top and bottom, which create a dipole moment effect,²⁵ influencing the surface and interface performance. On the contrary, the surface structure with the odd layers does not conform to stoichiometric chemical ratios; however, the same types of terminal atoms are present at the top and bottom, which eliminates the dipole moment effect between the top and bottom. In this study, the surface structure of TiN(111) with odd layers was adopted in the calculations to eliminate the dipole moment effect between the top and bottom caused by different types of terminal atoms. For a surface structure with odd layers, the terminal atoms can be N or Ti. If the terminal atoms are Ti atoms, the surface energy is calculated as

$$\gamma_{\text{surf-Ti}} = \left[E_{\text{slab}}^{\text{total}} - n_{\text{N}}E_{\text{TiN}}^{\text{bulk}} - (n_{\text{Ti}} - n_{\text{N}})E_{\text{Ti}}^{\text{bulk}} \right] / 2A. \quad (2)$$

If the terminal atoms are N atoms, the surface energy is calculated as

$$\gamma_{\text{surf-N}} = \left[E_{\text{slab}}^{\text{total}} - n_{\text{Ti}}E_{\text{TiN}}^{\text{bulk}} - (n_{\text{N}} - n_{\text{Ti}})E_{\text{N}}^{\text{atom}} \right] / 2A, \quad (3)$$

where $E_{\text{slab}}^{\text{total}}$, $E_{\text{TiN}}^{\text{bulk}}$, $E_{\text{Ti}}^{\text{bulk}}$, $E_{\text{N}}^{\text{atom}}$, n_{Ti} , and n_{N} denote the total energy of the TiN(111) surface structure, energy of the TiN unit cells, energy of each Ti atom in Ti unit cells, energy of N atoms, and the number of Ti atoms and N atoms in the surface structure, respectively.

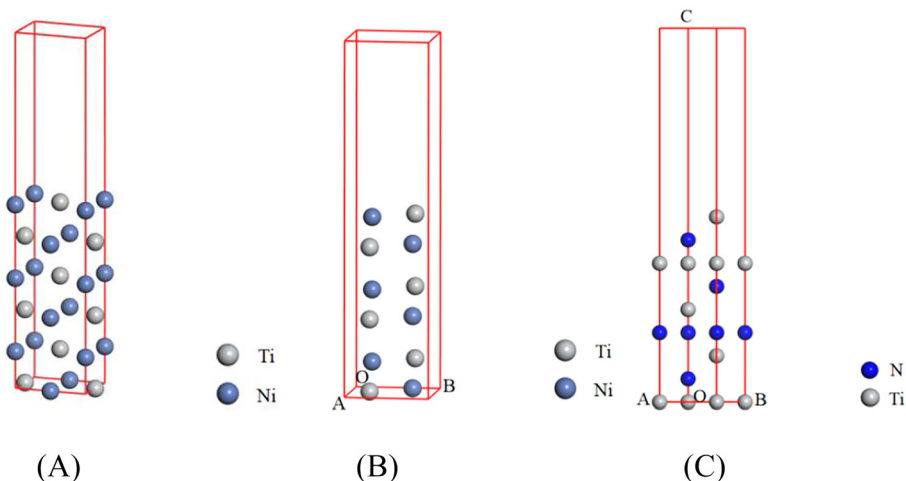


FIGURE 1 Three surface structures: (A) B2-NiTi(110), (B) B19'-NiTi(010), and (C) TiN(111)

The surface energies of B2-NiTi(110), B19'-NiTi(010), and TiN(111) with different layers of atoms were calculated using Equations 1–3 and shown in Table 2. The surface energy of B2-NiTi(110) starts to converge when the number of layers of atoms is >4. The surface energy was approximately 1.60 J/m² when there were four layers of atoms, which is similar to the surface energy of B2-NiTi(110) calculated by Guda Vishnu and Strachan.²⁶ For the B19'-NiTi(010) structure, the surface energy converges at 2.20 J/m² when the number of atomic layers is >6. When the number of atomic layers is >7, the surface energy of TiN(111) with two different terminals starts to converge, and the surface energy converges at 5.05 and 1.68 J/m² for surfaces with N and Ti atomic terminals, respectively. Furthermore, these results are similar to those calculated by Liu et al.²⁷ (4.89 and 1.69 J/m²). Considering the calculation efficiency and precision, in the current study, when the interface mode was constructed, the layers of atoms for B2-NiTi(110), B19'-NiTi(010), and TiN(111) were set to 4, 6, and 7, respectively (Table 2).

Work of fracture indicates the resistance of an interface to crack propagation. According to the Griffith fracture theory,^{28,29} if the work of fracture, G , is greater than the adhesion of work for an interface, W_{ad} ($G > W_{ad}$), there will be cracks on the interface; if $G < W_{ad}$, there will be cracks within the substrate or coating. The G of a material is expressed as $G \approx 2\gamma_{surf}$. The G of the crystal surfaces of B2-NiTi(110) and B19'-NiTi(010) can be calculated using γ_{surf} at the time of the convergence of the layers. The G of the crystal surface of TiN(111) can be expressed as the sum of the surface energies of the two structures with Ti and N as terminals at the time of convergence of layers,

that is, $G \approx (\gamma_{surf-Ti} + \gamma_{surf-N})$. The work of fracture of B2-NiTi(110), B19'-NiTi(010), and TiN(111) is listed in Table 2.

In the surface structure of B2-NiTi(110) and B19'-NiTi, every two layers of atoms are considered a repeating periodic structure (Figure 2). In the B2-NiTi(110) structure, the surface terminals with 2 N and 2 Ti, and that with 4 Ni and 1 Ti, are denoted as AI and AII,

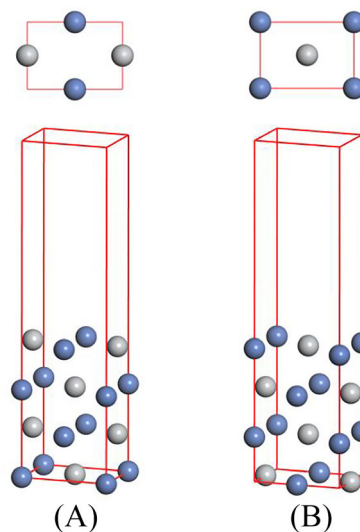


FIGURE 2 Surface structure of B2-NiTi(110) with four layers of atoms: Types of surface terminal atoms—(A) AI and (B) AII

TABLE 2 Surface energy and work of fracture of B2-NiTi(110), B19'-NiTi(010), and TiN(111) with different layers

Type of slab	Number of atomic layers (n)	Surface energy (J/m ²)		Work of fracture (J/m ²)
B2-NiTi(110)	1	2.17		3.2
	2	1.63		
	3	1.71		
	4	1.60		
	5	1.66		
	6	1.58		
	7	1.62		
	8	1.61		
B19'-NiTi(010)	2	2.14		4.4
	4	2.19		
	6	2.20		
	8	2.20		
	10	2.20		
TiN(111)		N-terminated	Ti-terminated	6.73
	3	7.70	1.78	
	5	6.27	1.86	
	7	5.05	1.68	
	9	5.11	1.74	
	11	5.05	1.69	

respectively (Figure 2). For the surface structure of B19'-NiTi, the atomic terminals are 1 Ni or 1 Ti (Figure 3), and they are denoted as MI and MII, respectively. In the surface structure of TiN(111), six layers of atoms constitute a repeating periodic structure. Therefore, there are six different types of atomic terminals in the surface structure of TiN(111) with seven layers of atoms, as shown in Figure 4; they are denoted as NI, NII, NIII, TII, TIII, and TIIII, respectively.

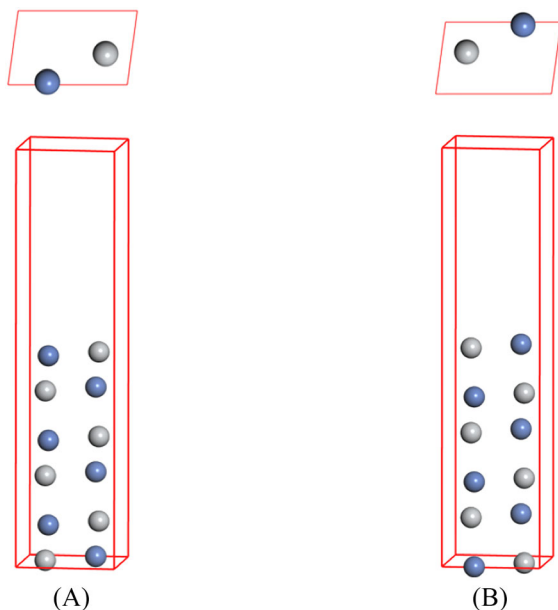


FIGURE 3 Surface structure of B19'-NiTi(010) with six layers of atoms: Types of surface terminal atoms—(A) MI and (B) MII

3.2 | Structure and work of adhesion of the interface

As discussed in Section 3.1, B2-NiTi(110) exhibits two types of terminal atoms (AI and AII) that are similar to those of B19'-NiTi(010) (MI and MII). However, the TiN(111) surface exhibits six types of terminal atoms (NI, NII, NIII, TII, TIII, and TIIII). Therefore, both B2-NiTi(110) and B19'-NiTi(010) can be combined with TiN(111) to form 12 different types of interface structures. If the interface structure is a combination of the AI and NI types, the interface structure was named AI-NI; the same naming approach was applied for all other interface structures, such as AI-NII, AII-NI, and AII-TIII.

However, as shown in Figures 2 and 4, B2-NiTi(110) and TiN(111) did not match each other because their macroshapes were rectangular and rhombic, respectively. Therefore, in interface structuring, the surface of TiN(111) required restructuring into a rectangular structure. The surface lattice parameters of B2-NiTi(110) were $a_1 = 3.011 \text{ \AA}$ and $b_1 = 4.258 \text{ \AA}$; after restructuring, the surface lattice parameters of TiN(111) were $a_2 = 3.003 \text{ \AA}$ and $b_2 = 5.202 \text{ \AA}$. Supercell expansion was required, because the mismatch degree of the 'a' lattice was 0.27% and that of the 'b' lattice was greater than 5%. B2-NiTi(110) was expanded by five times along the b axis, and TiN(111) was expanded by four times along the b axis. After supercell expansion, the lattice parameter of B2-NiTi(110) was $b_1 = 21.29 \text{ \AA}$ and that of TiN(111) was $b_2 = 20.808 \text{ \AA}$; the mismatch degree of the lattice was 2.26%, which conformed to the requirements.

Additionally, as shown in Figures 3 and 4, B19'-NiTi(010) and TiN(111) did not match with each other, because their macroshapes were rhomboid and rhombic, respectively. Therefore, the macroshapes of both ought to be restructured into a rectangular structure before

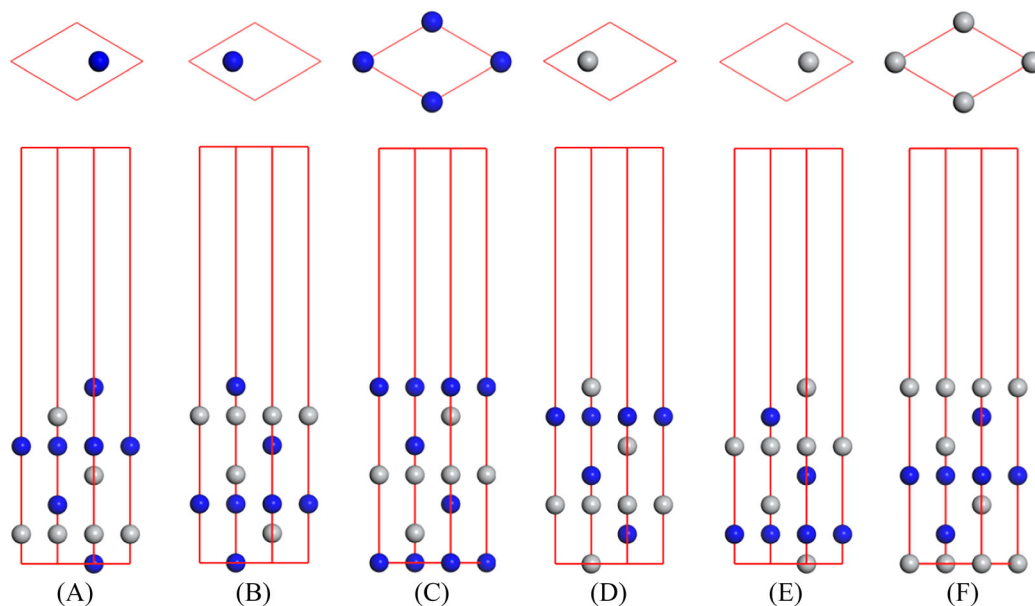


FIGURE 4 Surface structure of TiN(111) with seven layers of atoms: Types of surface terminal atoms—(A) NI, (B) NII, (C) NIII, (D) TII, (E) TIII, and (F) TIIII

interface construction. After restructuring, the surface lattice parameters of B19'-NiTi(O10) were $a_1 = 2.898 \text{ \AA}$ and $b_1 = 18.417 \text{ \AA}$, and those of TiN(111) were $a_2 = 3.003 \text{ \AA}$ and $b_2 = 5.202 \text{ \AA}$. The mismatch degree of the a-axis lattice was 3.5%, which conformed to the standard; the mismatch degree of the b-axis lattice was greater than 5%, and therefore, supercell expansion was required. The unit cell of B19'-NiTi(O10) was expanded by 1×2 times along the b axis, and that of TiN(111) was expanded by 1×7 times. After supercell expansion, the lattice parameter of B19'-NiTi(O10) was $b_1 = 36.834 \text{ \AA}$ and that of TiN(111) was $b_2 = 36.414 \text{ \AA}$; the mismatch degree of the lattice was 1.15%, which conformed to the requirements.

A universal binding energy relation (UBER³⁰) was adopted to obtain an appropriate interplanar spacing, d_0 , when an interface structure was constructed through the combination of B2-NiTi(110) or B19'-NiTi(O10) with TiN(111). The key point of this method was to provide the W_{ad} - d_0 relationship curve, firstly. W_{ad} refers to the adhesion work of interface when the interplanar spacing was set to d_0 . W_{ad} was calculated without optimizing the geometric structure interface model. Figure 5 shows a typical W_{ad} - d_0 curve, in which the d_0 at the point with the greatest work of adhesion was used as the initial interplanar spacing while constructing the interface. Then, the geometric structure of the interface was optimized, and the optimal interplanar spacing d_e and W_{ad} of the interface were calculated. Using the same method, the optimal spacing and work of adhesion of all possible interfaces in the two categories of TiN(111)//B2-NiTi(110) and TiN(111)//B19'-NiTi(O10) interfaces were calculated; all the related results are listed in Tables 3 and 4, respectively.

The work of adhesion was calculated using the following equation³¹:

$$W_{ad} = \frac{E_{slab}^a + E_{slab}^b - E_{a/b}}{A}, \quad (4)$$

where E_{slab}^a and E_{slab}^b represent the total energies of surface structure a and surface structure b after optimization, respectively; $E_{a/b}$ denotes

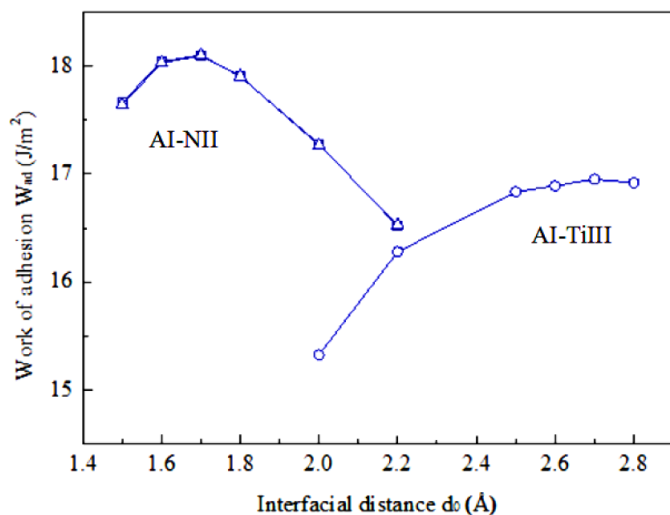


FIGURE 5 W_{ad} - d_0 relationship curve of Al-NiII and Al-TiIII

the total energy of the a/b interface structure; and A denotes the area of the interface; 'a' indicates B2-NiTi(110) or B19'-NiTi(O10), and 'b' indicates TiN(111).

The work of adhesion is an important parameter for measuring the bonding property and predicting the mechanical properties of the interface. The greater the work of adhesion, the stronger the bonding strength, and the more stable the interface structure. The work of adhesion for TiN(111)//B2-NiTi(110) interfaces was 4.63–4.66 J/m² (Table 3), when the terminal atoms were Ti on the TiN(111) side.

TABLE 3 Work of adhesion (W_{ad}) and interfacial separation (d_0 , d_e) before and after the geometry optimization of TiN(111)//B2-NiTi(110)

Interface model	UBER		Geometry optimization	
	d_0 (Å)	W_{ad} (J/m ²)	d_e (Å)	W_{ad} (J/m ²)
AI-TiI	2.70	16.96	2.41	4.66
AI-NI	1.70	18.11	1.57	5.47
AI-TiII	2.70	16.96	2.54	4.63
AI-NII	1.70	18.11	1.43	5.48
AI-TiIII	2.70	16.95	2.50	4.64
AI-NIII	1.70	18.09	1.91	5.29
AII-TiI	2.70	16.96	2.34	4.66
AII-NI	1.70	18.10	1.57	5.46
AII-TiII	2.70	16.96	2.48	4.64
AII-NII	1.70	18.10	1.49	5.49
AII-TiIII	2.70	16.95	2.50	4.65
AII-NIII	1.70	18.09	1.61	5.45

Abbreviation: UBER, universal binding energy relation.

TABLE 4 Work of adhesion (W_{ad}) and interfacial separation (d_0 , d_e) before and after the geometry optimization of TiN(111)//B19'-NiTi(O10)

Interface model	UBER		Geometry optimization	
	d_0 (Å)	W_{ad} (J/m ²)	d_e (Å)	W_{ad} (J/m ²)
MI-TiI	3.00	17.21	2.71	15.78
MI-NI	1.70	19.09	1.68	17.42
MI-TiII	3.00	17.21	2.80	15.79
MI-NII	1.70	19.11	1.38	17.47
MI-TiIII	3.00	17.21	2.80	15.78
MI-NIII	1.70	19.10	1.39	17.36
MII-TiI	3.00	17.21	2.79	15.79
MII-NI	1.70	19.12	1.40	17.36
MII-TiII	3.00	17.21	2.77	15.78
MII-NII	1.70	19.10	1.54	17.33
MII-TiIII	3.00	17.20	2.86	15.40
MII-NIII	1.70	19.11	1.61	17.35

Abbreviation: UBER, universal binding energy relation.

However, when the terminal atoms were N on the TiN(111) side, the work of adhesion increased by 0.6–0.8 eV, compared with that of the former. Furthermore, there is only a marginal difference in the work of adhesion between the TiN(111) interface with the same terminal atoms and the B2-NiTi(110) interface with different terminal atoms (0.01–0.16 eV).

Figure 6 shows the typical interface structure of TiN(111)//B2-NiTi(110) with Ti and N as the terminal atoms on the TiN(111) side, that is, All-TiI and All-NII. A hollow-site stacking structure was formed at the All-NII interface, as shown in Figure 7. Ti atoms at the B2-NiTi(110) side were projected onto the hollow sites of the plane constituted by the three N atoms at the TiN(111) side, which appeared to be a tetrahedral-like structure. However, this structure was not founded at All-TiI interface. After the geometry optimization of the All-NII, the Ti atoms at the B2-NiTi(110) side shifted upward and approached the three N atoms on the TiN(111) side. In the hollow-site structure, before geometry optimization, the bond lengths of Ti–N were 2.852, 2.295, and 2.295 Å, which became 2.1, 2.015, and 2.052 Å after optimization, respectively, which are smaller than

the bond length of Ti–N in TiN bulk cell. Therefore, Ti atoms in the hollow-site structure can be inferred to probably bond with all three N atoms. Thus, more bonds were formed at the interface for the All-NII compared with All-TiI, which is the main reason for the higher work of adhesion of the All-NII interface.

Table 4 shows the work of adhesion of the TiN(111)//B19'-NiTi(010) interface structure. Additionally, the interface with the N atomic terminal on the TiN(111) side was higher than that of the interface with the Ti atomic terminal, which is similar to the B2-NiTi(110)//TiN(111) interfaces, which can be attributed to the formation of more Ti–N bonds between N atoms on the TiN(111) side and Ti atoms on the B19'-NiTi(010) side. The work of adhesion of B19'-NiTi(010)//TiN(111) interfaces was 15.4–17.5 J/m², which is far greater than that of B2-NiTi(110)//TiN(111) interfaces (4.64–5.49 J/m²); this is because more atoms participate in bonding at the B19'-NiTi(010)//TiN(111) interfaces, and the bonding becomes stronger. The analysis of the electronic structure of interfaces and Mulliken overlap populations can validate this observation.

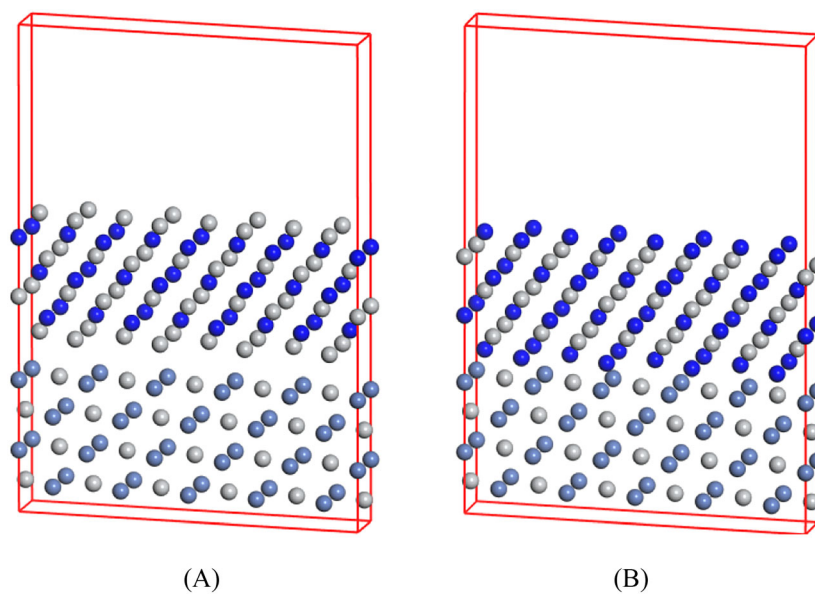


FIGURE 6 TiN(111)//B2-NiTi(110) interface models: (A) All-TiI and (B) All-NII

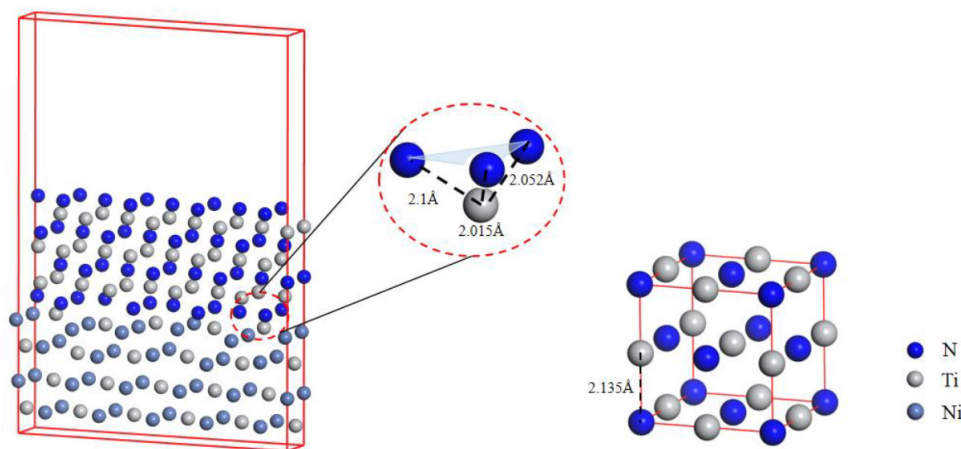


FIGURE 7 Hollow site of All-NII surface structure

The difference in the work of adhesion of the two interfaces suggested significant changes in the bonding strength of the TiN/NiTi interface when the NiTi substrate undergoes B2-B19' martensitic transformation. Both the shape memory and hyperelasticity properties of the NiTi alloys were closely related to the martensitic transformation. From the data in Tables 2–4, the work of adhesion of TiN(111)//B19'-NiTi(010) interface (between 15.4 and 17.5 J/m²) can be observed to be greater than the work of fracture of TiN(111) (6.73 J/m²); however, that of B2-NiTi(110)//TiN(111) interfaces (between 4.64 and 5.49 J/m²) was lower than the work of fracture of TiN(111) (6.73 J/m²). According to the Griffith fracture theory, these data indicate that fracture is prone to occur at the interface when NiTi substrate exhibits a B2 structure, whereas fracture is prone to occur in the coatings when the NiTi substrate transforms into the B19' structure.

3.3 | Charge density and Mulliken population of interfaces

Figure 8 shows the charge density distribution of the typical interface structure with Ti and N terminal atoms on the TiN side with B2-NiTi as the substrate, namely, AII-TiI and AII-NiI. In the AII-TiI interface structure, there is an overlap of electronic clouds between a small quantity of terminal Ti atoms on the TiN(111) surface and the terminal Ni atoms on the B2-NiTi(110) surface, which indicates the formation of a small number of covalent bonds at the interface. In the AII-NiI interface structure, there is an electron cloud overlap between almost all the terminal atoms N of the TiN(111) surface and the Ti of B2-NiTi(110). A large number of covalent bonds were formed at the interface, where the Ti atoms on one side of the interface were pulled toward

the N atoms on the other side of the interface. It thus follows from the charge density distribution that the structure at the AII-NiI interface was more tight and exhibited stronger binding performance than AII-TiI, which is consistent with the conclusion from the analyses of the work of adhesion and atomic structure.

Figure 9 shows the charge density of a typical interface structure with Ti and N as the terminal atoms on the TiN side with B19'-NiTi as the substrate (MI-NiI and MII-TiI). The bonding analysis results are similar to those of the AII-TiI and AII-NiI interfaces; there is a stronger bonding of the structure with the terminal N atoms on the TiN side.

The Mulliken overlap populations of AII-TiI, AII-NiI, MI-NiI, and MII-TiI interfaces were calculated to perform the quantitative analysis of bonding at the interface; the results are summarized in Tables 5 and 6. The overlap population can be used for the quantitative analysis of interactions among atoms. If the overlap population is positive, it indicates the existence of covalent bonds; the greater the value, the stronger the action of the covalent bond. If the overlap population is negative, it indicates an unstable structure, and the value possesses negligible relevance (not listed in Tables 5 and 6).

Table 5 shows that the main atoms participating in the formation of covalent bonds at the interface are Ti atoms on the TiN side and the Ni and Ti atoms on the B2-NiTi side for the AII-TiI structure. In Table 5, the digit in the name of the bond indicates the serial number of atoms in the interface structure model. For example, Ti 32–Ni 12 indicates a bond formed with No. Ti 32 on the TiN side and No. Ni 12 on the NiTi side at the interface. The calculation results show that there were eight bonds whose overlap population was positive, and the sum of the overlap population between Ni–Ti and Ti–Ti was 1.51 in the AII-TiI interface structure. For the AII-NiI interface structure, the main atoms participating in the formation of covalent bonds at the

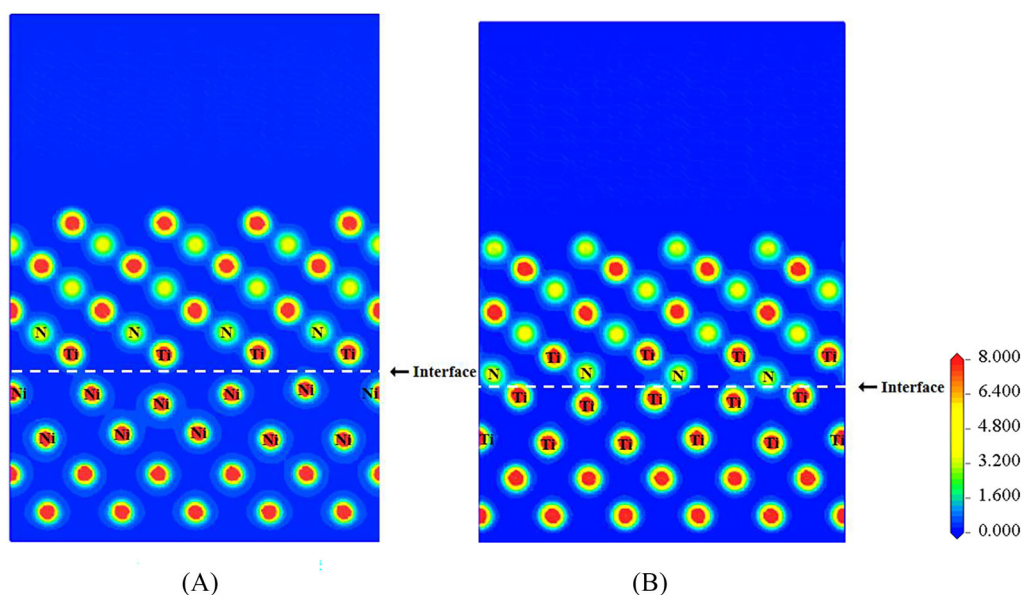


FIGURE 8 Electron density distributions of the two TiN(111)//B2-NiTi(110) interfaces along the (100) plane: (A) AII-TiI and (B) AII-NiI. The charge density is in the unit of $e/\text{Å}^3$

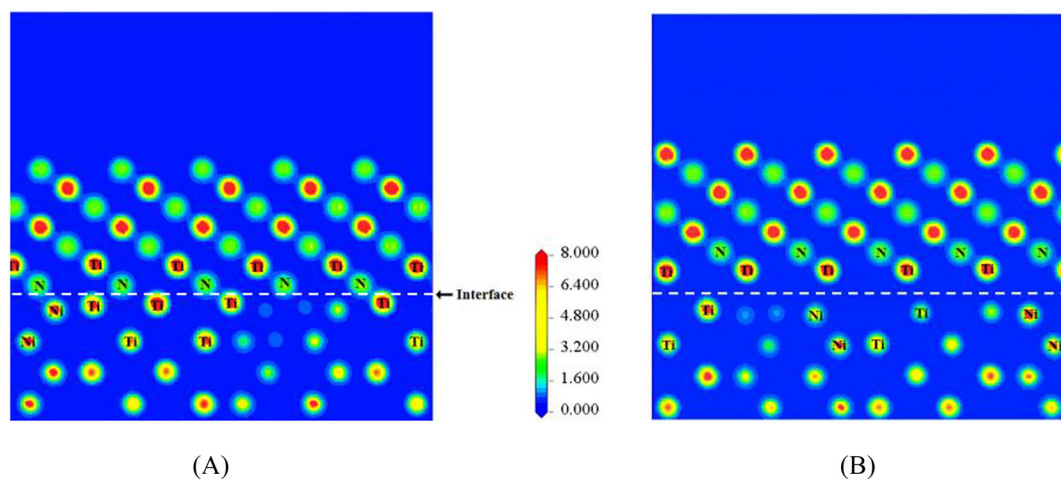


FIGURE 9 Charge density of the two TiN(111)//B19'-NiTi(110) interface structures: (A) MI-NiI and (B) MII-TiI. The charge density is in the unit of $e/\text{Å}^3$

TABLE 5 Overlapping population of the TiN(111)//B2-NiTi(110) surface

	Bond	Length (Å)	Population
Al-Ti	Ti 32—Ni 12	2.855	0.22
	Ti 40—Ni 16	2.839	0.13
	Ti 23—Ni 4	2.801	0.36
	Ti 24—Ni 8	2.613	0.22
	Ti 47—Ni 20	2.590	0.38
	Ti 20—Ti 48	2.902	0.11
	Ti 12—Ti 39	2.682	0.05
	Ti 8—Ti 31	2.648	0.04
Al-NiI	N 27—Ti 16	2.344	0.14
	N 27—Ti 20	2.177	0.30
	N 12—Ti 12	2.170	0.58
	N 4—Ti 4	2.094	0.66
	N 20—Ti 16	2.066	0.76
	N 28—Ti 20	2.015	0.79
	N 19—Ti 12	1.958	0.30
	N 3—Ti 4	1.916	0.42
N 11—Ti 8	1.861	0.48	

interface were N atoms on the TiN side and Ti atoms on the B2-NiTi side. There were nine bonds whose overlap population was positive, and the sum of the overlap population between Ti—N at the interface was 4.43. The overlap population results suggest that the interaction among atoms at the interface of Al-NiI was stronger than that at Al-TiI, which is consistent with the conclusion from the charge density analysis.

Table 6 shows that the main atoms participating in the formation of covalent bonds at the interface were N and Ti atoms on the TiN and B19'-NiTi sides, respectively, at the interface for the MI-NiI interface structure. There were 14 bonds whose overlap population was

TABLE 6 Overlapping population of the TiN(111)//B19'-NiTi (010) surface

	Bond	Length (Å)	Population
MI-NiI	N 51—Ti 36	1.844	0.51
	N 3—Ti 9	1.876	0.45
	N 12—Ti 11	1.914	0.41
	N 36—Ti 34	1.944	0.76
	N 11—Ti 10	1.959	0.81
	N 44—Ti 35	1.985	0.38
	N 28—Ti 33	1.999	0.87
	N 35—Ti 34	2.024	0.31
	N 20—Ti 12	2.035	0.79
	N 43—Ti 35	2.041	0.42
	N 19—Ti 11	2.057	0.58
	N 4—Ti 10	2.076	0.32
	N 52—Ti 36	2.112	0.48
	N 27—Ti 12	2.232	0.20
MII-TiI	Ti 59—Ni 22	2.959	0.28
	Ti 67—Ni 23	2.979	0.24
	Ti 21—Ti 52	2.906	0.21
	Ti 46—Ti 91	2.914	0.20
	Ti 24—Ti 75	2.943	0.33
	Ti 48—Ti 100	2.961	0.24
	Ti 23—Ti 68	2.969	0.19
	Ti 22—Ti 60	2.983	0.20

positive, and the sum of overlap was 7.29. For the MII-TiI interface structure, the main atoms participating in the formation of covalent bonds at the interface were Ti atoms on the TiN side and Ni and Ti atoms on the NiTi side. There were nine bonds whose overlap population was positive, and the sum of the overlap population between Ni, and Ti and Ti—Ti was 1.89. Therefore, the interaction among atoms at

the interface of MI–NII was stronger than that of MII–Til; furthermore, there were more covalent bonds, which is consistent with the conclusion from the charge density analysis. The comparison between Tables 5 and 6 reveals that both the bonding strength and the number of bonds were greater in the interface structure formed with B19'–NiTi as substrate than those with B2–NiTi as substrate. This explains why the work of adhesion of the B19'–NiTi(010)//TiN(111) interface is greater than that of the B2–NiTi(110)//TiN(111) interface.

4 | CONCLUSION

In this study, the background behind the application of NiTi alloy instruments modified with TiN films was targeted, and the TiN(111) interface was combined with B2–NiTi(110) and B19'–NiTi(010) to construct two interface models: TiN(111)//B2–NiTi(110) and TiN(111)//B19'–NiTi(010), respectively. The atomic configuration, electronic structure, and work of adhesion of TiN(111)//B2–NiTi(110) and TiN(111)//B19'–NiTi(010) interfaces were investigated by using a first-principles method based on the DFT.

The following conclusions can be drawn from this study:

1. A hollow-site stacking structure was formed in the interface when Ti and N were the terminal atoms on two sides, which demonstrated a stronger bonding performance and greater thermodynamic stability, compared with the other interfaces with Ni and Ti as the terminal atoms.
2. The work of adhesion of the TiN(111)//B19'–NiTi(010) interfaces was far greater than that of the TiN(111)//B2–NiTi(110) interfaces, which indicates that the martensitic transformation significantly influences the interfacial bonding strength of TiN/NiTi interfaces under the stress or the temperature.
3. The work of adhesion of the TiN(111)//B19'–NiTi(010) (17.47 J/m²) was larger than that of TiN(111)//B2–NiTi(110) (5.49 J/m²), which was smaller than the work of fracture of TiN(111) (6.73 J/m²). According to the Griffith fracture theory, under the influence of external force, cracks easily occur at the interface of a B2 structure; however, when NiTi is transformed into the B19' structure, the cracks were prone to occur within the coated thin film layer.
4. The calculated Mulliken overlap population results of the two interface structures suggested that more atoms were contributing to bonding at the TiN(111)//B19'–NiTi(010) interfaces, ultimately strengthening the bonding. This could explain why the work of adhesion of the TiN(111)//B19'–NiTi(010) interfaces is greater than that of the TiN(111)//B2–NiTi(110) interfaces.

The above result can help us understand the changes in the film/NiTi interface structure and the bonding performance of NiTi before and after martensitic transformation, which is significantly important for the service reliability analysis of TiN films modified NiTi alloy devices.

ACKNOWLEDGMENT

This work was supported by the Natural Science Foundation of Sichuan Province, China (2022NSFSC0292).

DATA AVAILABILITY STATEMENT

The data that support the findings of this study are available from the corresponding authors upon reasonable request.

ORCID

Dong Xie  <https://orcid.org/0000-0003-0902-8117>

REFERENCES

1. Petrini L, Migliavacca F. Biomedical applications of shape memory alloys. *J Metall.* 2011;2011:1–15. doi:10.1155/2011/501483
2. Kahn H, Huff MA, Heuer AH. The TiNi shape-memory alloy and its applications for MEMS. *J Micromech Microeng.* 1998;8(3):213–221. doi:10.1088/0960-1317/8/3/007
3. Nazarenko AI. Technique and some results of space debris penetration probability estimate for Russian modules of ISS[Z], Proceedings of the 17th IADC Meeting, Darmstadt, Germany; 1999.
4. Kheirikhah MM, Rabiee S, Edalat ME. A review of shape memory alloy actuators in robotics. In: Ruiz-Del-Solar J, Chown E, Plöger PG, eds. *Lecture Notes in Computer.* Berlin, H: Science Springer.
5. Huang J, Dong P, Hao W, et al. Biocompatibility of TiO₂ and TiO₂/heparin coatings on NiTi alloy. *Appl Surf Sci.* 2014;313:172–182. doi:10.1016/j.apsusc.2014.05.182
6. Aun DP, Houmard M, Mermoux M, et al. Development of a flexible nanocomposite TiO₂ film as a protective coating for bioapplications of superelastic NiTi alloys. *Appl Surf Sci.* 2016;375:42–49. doi:10.1016/j.apsusc.2016.03.064
7. Jin S, Zhang Y, Wang Q, Zhang D, Zhang S. Influence of TiN coating on the biocompatibility of medical NiTi alloy. *Colloids Surf B Biointerfaces.* 2013;101:343–349. doi:10.1016/j.colsurfb.2012.06.029
8. Yang S, Zhou F, Xiao T, et al. Surface modification with SiO₂ coating on biomedical TiNi shape memory alloy by sol-gel method. *Trans Nonferrous Met Soc Chin.* 2015;25(11):3723–3728. doi:10.1016/S1003-6326(15)64015-8
9. Meisner SN, Yakovlev EV, Semin VO, et al. Mechanical behavior of Ti-Ta-based surface alloy fabricated on TiNi SMA by pulsed electron-beam melting of film/substrate system. *Appl Surf Sci.* 2018;437:217–226. doi:10.1016/j.apsusc.2017.12.107
10. Otsuka K, Ren X. Physical metallurgy of Ti–Ni-based shape memory alloys. *Prog Mater Sci.* 2005;50(5):511–678. doi:10.1016/j.pmatsci.2004.10.001
11. Dong X, Fei Y, Wang JB, et al. Deformation behavior of TiO₂ films deposited on NiTi shape memory alloy after tensile and water-bath heating tests. *Surf Coat Technol.* 2021;416:127151. doi:10.1016/j.surfcoat.2021.127151
12. Chen L, Li Y, Xiao B, et al. First-principles calculation on the adhesion strength, fracture mechanism, interfacial bonding of the NiTi(111)//α–Al₂O₃(0001) interfaces. *Mater Des.* 2019;183:108119. doi:10.1016/j.matdes.2019.108119
13. Hong-Li W, Xin-Qing Z, Sheng-Kai G. Effect of Nb doping on electronic structure of TiO₂/NiTi interface: a first-principle study. *Acta Phys Sin.* 2008;57(12):7794–7799. doi:10.7498/aps.57.7794
14. Li GF, Zheng HZ, Shu XY, Peng P. Structural stability of characteristic interface for NiTi/Nb nanowire: first-principle study. *Met Mater Int.* 2015;22(1):1–6. doi:10.1007/s12540-015-5367-9
15. Segall MD, Lindan PJD, Probert MJ, et al. First-principles simulation: ideas, illustrations and the CASTEP code. *J Phys Condens Matter.* 2002;14(11):2717–2744. doi:10.1088/0953-8984/14/11/301

16. Cuevas F, Latroche M, Bourée-Vigneron F, Percheron-Guégan A. A conjoint XRD–ND analysis of the crystal structures of austenitic and martensitic $\text{Ti}_{0.64}\text{Zr}_{0.36}\text{Ni}$ hydrides. *J Solid State Chem.* 2006;179(11):3295–3307. doi:[10.1016/j.jssc.2006.06.025](https://doi.org/10.1016/j.jssc.2006.06.025)
17. Kudoh Y, Tokonami M, Miyazaki S, Otsuka K. Crystal structure of the martensite in Ti–49.2 at.%Ni alloy analyzed by the single crystal X-ray diffraction method. *Acta Metall.* 1985;33(11):2049–2056. doi:[10.1016/0001-6160\(85\)90128-2](https://doi.org/10.1016/0001-6160(85)90128-2)
18. Aigner K, Lengauer W, Rafaja D, Ettmayer P. Lattice parameters and thermal expansion of Ti (C_xN_{1-x}), Zr (C_xN_{1-x}), Hf (C_xN_{1-x}) and TiN_{1-x} , from 298 to 1473 K as investigated by high-temperature X-ray diffraction. *J Alloys Compd.* 1994;215(1–2):121–126. doi:[10.1016/0925-8388\(94\)90828-1](https://doi.org/10.1016/0925-8388(94)90828-1)
19. Yu F, Liu Y. First-principles calculations of structural, mechanical, and electronic properties of the B2-phase NiTi shape-memory alloy under high pressure. *Comput Secur.* 2019;7(4):57–70. doi:[10.3390/computation7040057](https://doi.org/10.3390/computation7040057)
20. Strutt ER, Radetic T, Olevsky EA, Meyers MA. Combustion synthesis/quasi-isostatic pressing of $\text{TiC}_{0.7}$ –NiTi cermets: microstructure and transformation characteristics. *J Mater Sci.* 2008;43(17):5905–5923. doi:[10.1007/s10853-008-2848-y](https://doi.org/10.1007/s10853-008-2848-y)
21. Šesták P, Cerný M, Pokluda J. Elastic properties of B19' structure of NiTi alloy under uniaxial and hydrostatic loading from first principles. *Strength Mater.* 2008;40(1):12–15. doi:[10.1007/s11223-008-0004-1](https://doi.org/10.1007/s11223-008-0004-1)
22. Lazar P, Redinger J, Podloucky R. Density functional theory applied to VN/TiN multilayers. *Phys Rev B.* 2013;76(17):174112. doi:[10.1103/PhysRevB.76.174112](https://doi.org/10.1103/PhysRevB.76.174112)
23. Kutschej K, Rashkova B, Shen J, Edwards D, Mitterer C, Dehm G. Experimental studies on epitaxially grown TiN and VN films. *Thin Solid Films.* 2007;516(2–4):369–373. doi:[10.1016/j.tsf.2007.06.104](https://doi.org/10.1016/j.tsf.2007.06.104)
24. Pang X, Yang W, Yang J, Pang M, Zhan Y. Atomic structure, stability and electronic properties of $\text{S}(\text{Al}_2\text{CuMg})/\text{Al}$ interface: a first-principles study. *Intermetallics.* 2018;93:329–337. doi:[10.1016/j.intermet.2017.10.014](https://doi.org/10.1016/j.intermet.2017.10.014)
25. Han Y, Dai Y, Shu D, Wang J, Sun B. First-principles study of $\text{TiB}_2(0001)$ surfaces. *J Phys Condens Matter.* 2006;18(17):4197–4205. doi:[10.1088/0953-8984/18/17/008](https://doi.org/10.1088/0953-8984/18/17/008)
26. Guda Vishnu K, Strachan A. Size effects in NiTi from density functional theory calculations. *Phys Rev B.* 2012;85(1):014114. doi:[10.1103/PhysRevB.85.014114](https://doi.org/10.1103/PhysRevB.85.014114)
27. Liu C, Jin N, Li Z, Liu X. First-principles calculations on the electronic structure and bonding nature of TaN(111)/TiN(111) interface. *J Alloys Compd.* 2017;717(717):326–332. doi:[10.1016/j.jallcom.2017.05.033](https://doi.org/10.1016/j.jallcom.2017.05.033)
28. Kelly A, Macmillan NH. *Strong Solids.* Oxford: Clarendon Press; 1986.
29. Li Y, Gao Y, Xiao B, Min T, Ma S, Yi D. Theoretical calculations on the adhesion, stability, electronic structure, and bonding of Fe/WC interface. *Appl Surf Sci.* 2011;257(13):5671–5678. doi:[10.1016/j.apsusc.2011.01.072](https://doi.org/10.1016/j.apsusc.2011.01.072)
30. Rose JH, Ferrante J, Smith JR. Universal binding energy curves for metals and bimetallic interfaces. *Phys Rev Lett.* 1981;47(9):675–678. doi:[10.1103/PhysRevLett.47.675](https://doi.org/10.1103/PhysRevLett.47.675)
31. Na J, Yang Y, Jian L, et al. First-principles calculation on $\beta\text{-SiC}(111)/\alpha\text{-WC}(0001)$ interface. *J Appl Phys.* 2014;115(22):5811–5836. doi:[10.1063/1.4883758](https://doi.org/10.1063/1.4883758)

How to cite this article: Xie D, Wang X, Wei L, et al. Atomic configuration, electronic structure, and work of adhesion of TiN(111)//B2-NiTi(110) and TiN(111)//B19'-NiTi(010) interfaces: Insights from first-principles simulations. *Surf Interface Anal.* 2022;1–11. doi:[10.1002/sia.7158](https://doi.org/10.1002/sia.7158)